Effect of Shear Flow on the Formation of Ring-Shaped ABA Amphiphilic Triblock Copolymer Micelles

Haizhou Yu and Wei Jiang*

State Key Laboratory of Polymer Physics and Chemistry, Changchun Institute of Applied Chemistry, Chinese Academy of Sciences, Changchun 130022, Graduate School of the Chinese Academy of Sciences, P. R. China

Received October 21, 2008; Revised Manuscript Received March 18, 2009

ABSTRACT: We have investigated the effect of shear flow on the formation of ring-shaped ABA triblock copolymer ($P4VP_{43}$-*b*-PS_{260}-*b*-$P4VP_{43}$) micelles. The results reveal that shear flow plays an important role in the formation of the rings. Both ring size and its distribution are found to be dependent sensitively on the stirring rate. Sizable rings are more likely to be formed at moderate stirring rate. Interestingly, the ring formation mechanism is also dependent on the shear flow. Copolymers are likely to form rings via end-to-end cylinder connection at low stirring rates, whereas they tend to form rings via the pathway of the rod−sphere−vesicle−ring at high stirring rates.

Introduction

The self-assembly of block copolymers has been an interesting subject for many years.[1−5] Amphiphilic block copolymers can self-assemble into various micelles.[6−8] These micelles have received much attention because of their potential applications in such fields as drug delivery, cosmetics, electronics, advanced materials, and so on.[9−11] Recently, ring-shaped micelles, in particular, have become attractive due to their special configuration.[8,12] Much research has been performed to investigate the formation mechanism of the ring-shaped micelles. For instance, He et al. proposed a pathway for the formation of ring-shaped micelles using the simulation method in which the spherical micelles first grow into small disks and then into a hole, which nucleates at the center of the disks, and finally, the perforated disks evolve into rings.[13] Another mechanism, for instance, end-to-end connection, theoretically predicts the formation of rings in cylindrical micelles and has been partially observed experimentally.[14−16]

On the other hand, the effect of shear flow on the phase behavior of amphiphilic systems, including diblock copolymers, surfactants, and liquid crystals, has attracted considerable attention both for its importance in basic research and in practical application.[17−19] Koppi et al. reported the clear experimental evidence of the shear induced order in symmetric diblock copolymer poly(ethylene−propylene)−poly(ethythylene) (PEP−PEE) melts under reciprocating shear.[20] Soos et al. investigated the effect of shear rate on the aggregation and breakage of fully destabilized polystyrene particles under turbulent conditions.[21] In self-assembled surfactant systems, shear-induced isotropic sponge-to-lamellar phase transition was observed.[17,22,23] Stirring is usually applied in the preparation of a micellar solution.[24,25] However, the effect of shear flow on micelle formation remains unclear. In this paper, the self-assembly of the poly (4-vinypyridine)-*b*-polystyrene-*b*-poly (4-vinypyridine) ($P4VP_{43}$-*b*-PS_{260}-*b*-$P4VP_{43}$) triblock copolymer in dioxane/water mixtures into ring-shaped micelles is investigated by changing the stirring rate. The results reveal that shear flow not only affects ring size and its distribution, but also determines the formation mechanisms for ring-shaped micelles.

* Author to whom correspondence should be addressed. E-mail address: wjiang@ciac.jl.cn.

Experimental Section

Materials. The copolymer used in this study was a triblock copolymer of $P4VP_{43}$-*b*-PS_{260}-*b*-$P4VP_{43}$ (the numbers in the subscripts indicate the number of repeat units of the blocks) (M_n = 36000 g/mol, PDI = 1.09), which was purchased from Polymer Source Inc. Canada.

Preparation of the Micelles. The triblock copolymer (1 wt %) was directly dissolved in mixtures of dioxane (a common solvent for PS and P4VP blocks) and deionized water (a precipitator for PS blocks, 25 wt %). These solutions were kept stirred at different rates in a vitreous bottle with a magnetic stirrer at room temperature for 6 d (or for varying times for the kinetic studies). Then, five times the amount of the deionized water of the micellar solutions was added to quench the resulting micellar morphologies. Finally, the resulting solutions were placed in dialysis bags and dialyzed against distilled water for 4 d to remove organic solvents. The time between the copolymer was dissolved in the mixtures of dioxane and deionized water and the subsequent quintuple amount of water addition was named the annealing time. In the present work, morphological transition does not take place when the annealing time is beyond 24 h, but to make the results comparable with one another, the container and the sample volume, as well as the stirring bar, remained the same for all experiments.

Field Emission Scanning Electron Microscopy (SEM). SEM measurements were performed on an XL 30 E-SEM (FEG, Micrion FEI PHILIPS) operated at an acceleration voltage of 20kV. The dialyzed colloidal solutions were diluted by a factor of 10−20 to prepare the SEM samples. To prepare the samples for SEM, a drop of the very dilute micelle solution after dialysis was dropped onto the silicon (Si) wafers. Prior to coating, the silicon substrates were cleaned in a bath of 100 mL of 80% H_2SO_4, 35 mL of H_2O_2, and 15 mL of deionized water for 15 min at 80 °C and rinsed several times in deionized water. The silicon surface was then dried with compressed nitrogen gas. The coated substrates were then dried in air and at room temperature for 1 d to let the micelles set on the Si-wafer. Then, the samples were coated with a thin layer of gold (Au). The Au layer coating time and density for all of the samples were under the same condition to reduce the standard error of the measurement.

Transmission Electron Microscopy (TEM). Transmission electron microscope (TEM, JEOL JEM-1011 microscope, operating at an acceleration voltage of 100 kV) was also used to visualize the aggregates morphologies at room temperature. The dilute dialyzed samples were deposited on copper grids precoated with a thin polymer film and then coated with thin carbon film. After 15 min, excess solution was blotted away using a strip of filter paper.

10.1021/ma900107r CCC: $40.75
Published on Web 04/07/2009

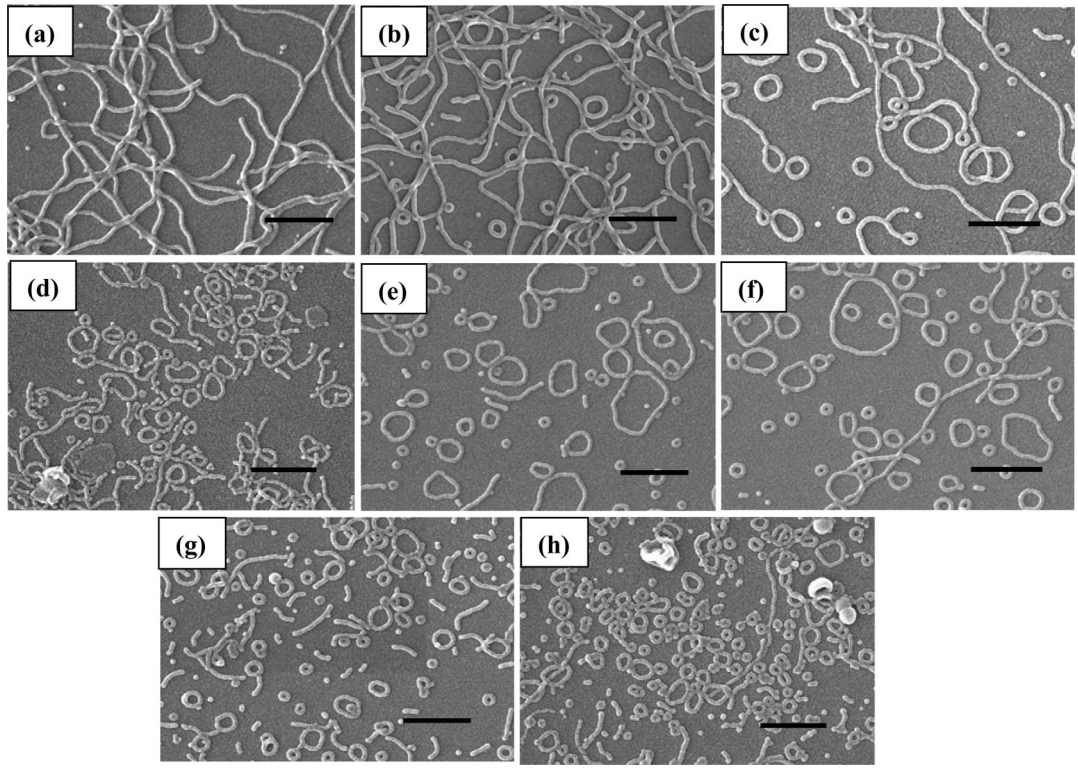

Figure 1. SEM images of $P4VP_{43}$-*b*-PS_{260}-*b*-$P4VP_{43}$ micellar aggregates prepared at different stirring rates in dioxane/water (25 wt % water content) mixtures: (a) 0, (b) 100, (c) 200, (d) 500, (e) 800, (f) 1000, (g) 1500, and (h) 2000 rpm. Annealing time for all solutions is 6 d. All solutions have the same initial copolymer concentration, i.e., 1 wt %. The bars represent 500 nm.

Scheme 1. Representations for the Measured Dimensions of the Ring and Cylinder

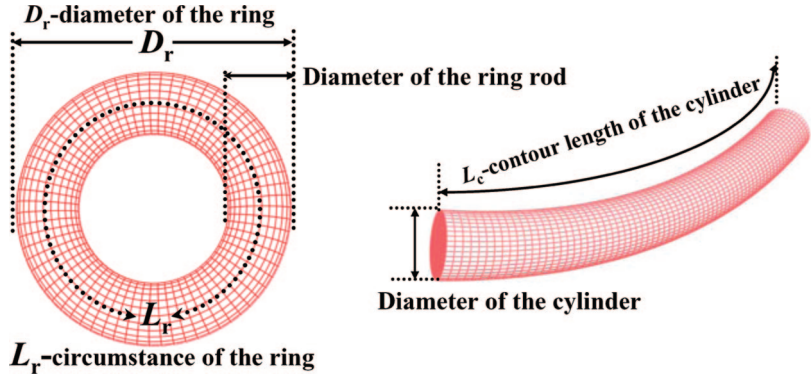

The samples were allowed to dry in the air and at room temperature for 1 d before observation.

Results and Discussion

Effect of Stirring Rate on the Ring-shaped Micelles Formation. Figure 1 presents the scanning electron microscopy (SEM) photographs of the aggregate morphologies formed at different stirring rates. The samples were extracted from different stirred solutions, respectively. It is clear that long cylindrical micelles (>3 μm) are formed without stirring (Figure 1a). The diameter of the visible part of the long cylinders was ca. 37 nm. Similar micelles have also been synthesized by Won et al.,[26] Liu et al.,[27] and Croce et al.[28] When stirring (100 rpm) was applied, the cylinders (ca. 2 μm) became the dominating morphologies coexisting with a minority of rings and long-tailed rings (Figure 1b). However, when the stirring rate was increased to 200 rpm, majority of the rings with a minority of cylinders (ca. 1 μm) appeared (Figure 1c). The average diameter of the rings was ca. 175 nm, and collected about 300 micelles from the SEM images. At higher stirring rates, i.e., 500, 800, 1000, 1500, and 2000 rpm, the rings became the dominant morphology (Figure 1d−h). Interestingly, sizable rings (ca. 220 nm) were obtained when the stirring rate was 800 rpm (Figure 1e). Smaller rings (ca. 130 nm) became of predominant morphology when the stirring rate reached 2000 rpm, as shown in Figure 1h. The results reveal that both the shape and the size of the micellar aggregates rely on the stirring rate. The measured dimensions of the ring and cylinder are shown in Scheme 1.

The average diameter of the rings (D_a) as a function of the stirring rate is given in Figure 2. It can be found that the diameter grows as the stirring rate is increased to 800 rpm. Thereafter, it decreases markedly with a further increase in the stirring rate. The average diameter of the ring decreased by ca. 90 nm when the stirring rate was amplified from 800 to 2000 rpm; however, the diameter of the ring rod remained unchanged, i.e. 34 nm. Notably, small rings could be found occasionally at low stirring rates. This is because the flow field in the solution is not uniform. The flow rate in some local regions is relatively

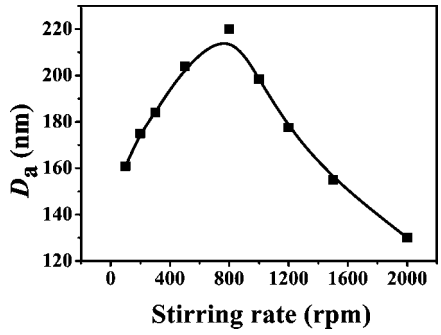

Figure 2. Average diameter of the rings (D_a) as a function of the stirring rate collected from SEM images.

high. Besides the ring size, the size distribution was also affected by the stirring rate. Figure 3 shows the ring size distributions at different stirring rates. It can be seen that the ring size distribution tended to become wider first and then narrower as the stirring rate increased.

To further study the effect of stirring rate on the micelles, we increased the stirring rate step by step up to 2000 rpm. Six steps, i.e. 0, 100, 500, 800, 1500, and 2000 rpm, were employed in this study. The stirring time at each step was 1 d. The samples were extracted from the same solution at different steps. Figure 4 displays the TEM images showing the aggregate morphologies at different steps. It can be seen that the results are quite similar to those in Figure 1. Without stirring, the copolymers form long cylinders (Figure 4a). It is noteworthy that the cylinders can remain unchanged for one month without any exoteric disturbance. However, these long cylinders change to the mixtures of cylinders and rings, then to predominant ring-shaped micelles with an increasing stirring rate, step by step, up to 2000 rpm (Figure 4b−f). Moreover, the ring diameters reach a maximum at the stirring rate of 800 rpm (Figure 4d). The results are quite consistent with those in Figure 1. This indicates that increasing stirring rate directly and increasing stirring rate step by step to a same stirring rate have similar effect on the aggregate morphology.

Ring Formation Mechanism at Low Stirring Rate. Ring formation mechanisms have been investigated by capturing the intermediate structures at different stages. The results of this study suggest the end-to-end cylinder connection as the dominating mechanism at low stirring rates to achieve sizable ring formation. Figure 5a-c provides direct visual evidence indicating ring formation through the end-to-end cylinder connection. Long cylindrical micelles (>3 μm) are formed at the first stage (Figure 5a) when the annealing time is 5 min. When annealing time is increased to 12 h, the cylinders become short (ca. 1 μm), and appear with many rings (Figure 5b). Then, the cylinders connect end-to-end, forming dominant rings when the annealing time is further increased to 24 h (Figure 5c). This process is depicted by the representation in Figure 5d-f. Moreover, we present the obtained ring circumference distribution and cylinder length distribution through Figure 5c. The results are also given in Figure 6. We can find that the two distributions are quite similar to one another. This result further supports the ring formation mechanism of the end-to-end cylinder connection. In addition, some branched cylinders (Figure 7a−c) were occasionally observed in the experiments. The end-to-end connection of the branched cylinders (in Figure 7a-c arrow pointed to) led to the formation of the complex rings as shown in (Figure 7d−h). Notably, the structures present in Figure 7 almost disappear if the stirring rate is higher than 1000 rpm.

Ring Formation Mechanisms at High Stirring Rate. It has been mentioned that bending energy increases as the radius of curvature decreases for ring structures.[29] Thus, the bending energy of the small rings (whose circumference is as small as 70 nm as shown in Figure 9a) is higher than that of the sizable rings (as big as 200 nm in Figure 6a).[15,29] We deduce that end-to-end connection is not the major method for small ring formation at high stirring rates because the two ends of a rod, especially for short rods, are difficult to connect to each other. Figure 8 presents another mechanism, such as the rod−sphere−vesicle−ring transition for small ring formation at high stirring rates. It provides direct visual evidence indicating ring formation at the stirring rate of 2000 rpm. Long cylinders (ca. 450 nm) are initially formed at the annealing time of 5 min (Figure 8a). Figure 8b indicates that the cylinders become short and break into spheres under vigorous stirring when annealing time is increased to 1 h. With a further increase in the annealing time to 10 h, most of the spheres become swollen (Figure 8c). And when the annealing time is increased to 15 h, mixtures of small rings and vesicles become the dominant morphologies (Figure 8d). The vesicular nature is evidenced from the TEM micrograph, which demonstrates higher transmission in the center of the aggregates than around their periphery. An enlarged vesicle micrograph is inserted on the top right corner of Figure 8d. At the last stage, the vesicles break up to form small rings (Figure 8e) when the annealing time is further increased to 24 h. The morphologies remain unchanged even when the annealing time is beyond 24 h. Moreover, end-to-end cylinder connection

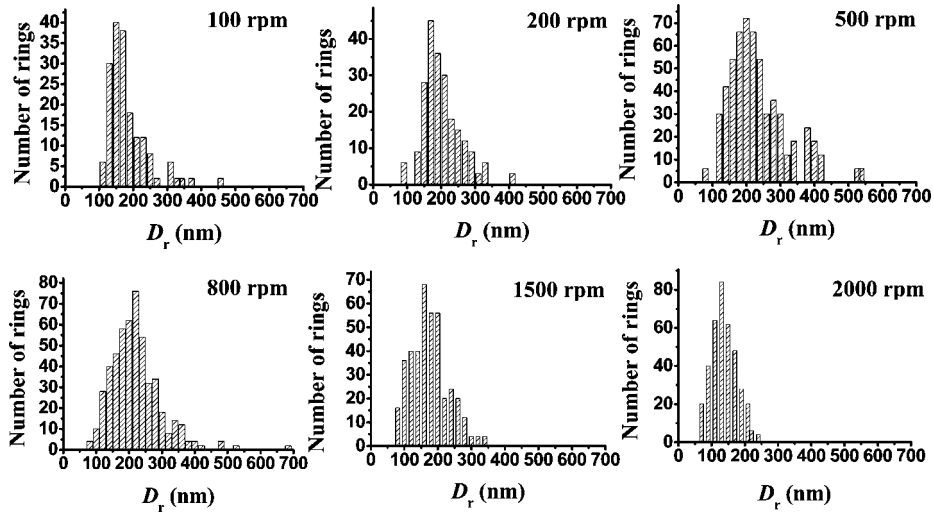

Figure 3. Ring size (D_r) distribution (histograms) at different stirring rates, collected from SEM images.

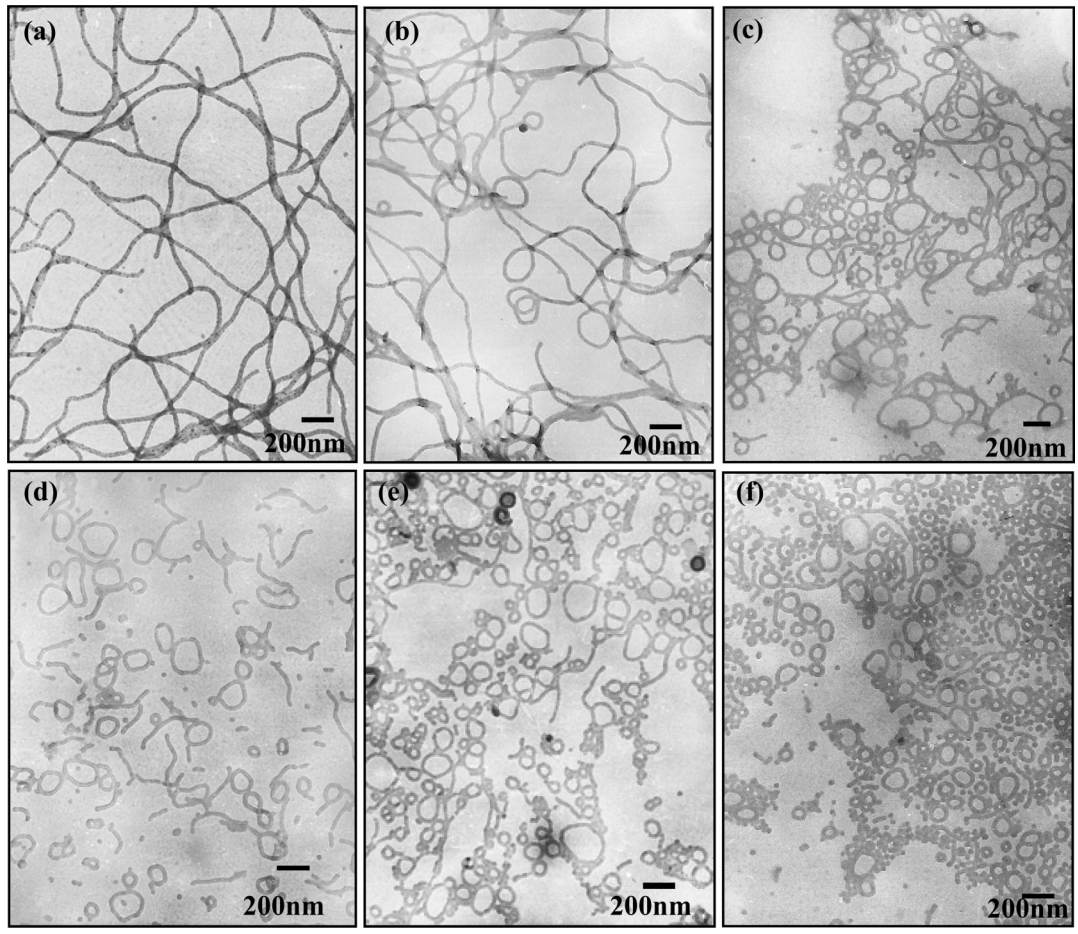

Figure 4. TEM images of the aggregate morphologies formed at different steps when the stirring rate is increased step by step from 0 to 2000 rpm: (a) 0, (b) 100, (c) 500, (d) 800, (e) 1500, and (f) 2000 rpm.

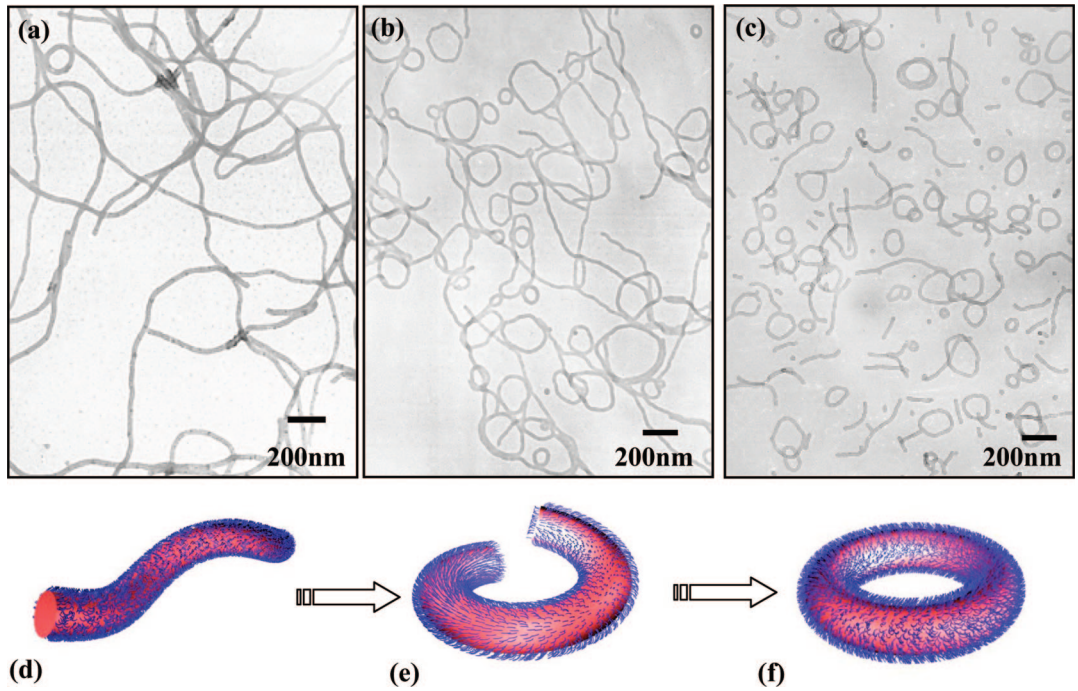

Figure 5. (a−c) TEM images of the aggregate morphologies trapped at different annealing times at a low stirring rate (200 rpm): (a) 5 min, (b) 12 h, (c) 24 h. (d−e) Representations for ring formation via end-to-end cylinder connection. Red represents the PS core, and blue represents the P4VP corona.

cannot be the primary formation mechanism of small rings at high stirring rates because the ring circumference in Figure 8e is much smaller than the length of the cylinders in Figure 8a (see the histograms in Figure 9). Furthermore, the ring circum-

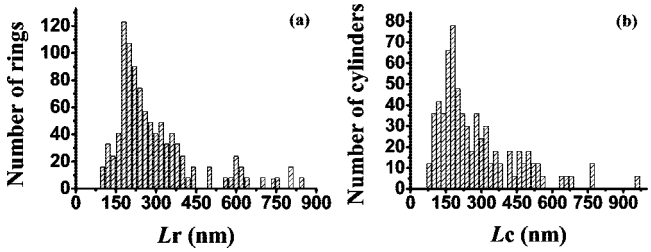

Figure 6. (a) Distribution of the ring circumferences (L_r) collected from Figure 5c. (b) Distribution of the cylinder lengths (L_c) collected from Figure 5c.

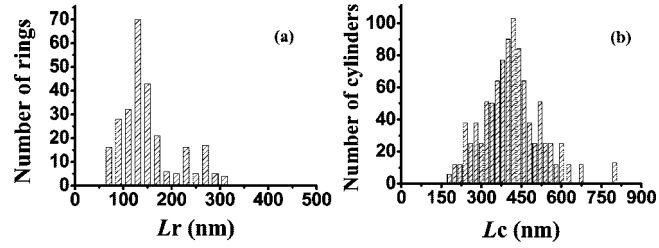

Figure 9. (a) Distribution of the ring circumferences (L_r) collected from Figure 8e. (b) Distribution of the cylinder contour lengths (L_c) collected from Figure 8a.

ference in Figure 8e has no coherence with the length of the cylinders trapped at the stirring rate of 2000 rpm in the experiments. For the purpose of clarity, the representations for small ring formation via the rod−sphere−vesicle−ring process are shown in Figure 8f-i.

The radius of the spherical micelle was 22 nm, which is quite close to that (21 nm) of the end-cap of the cylinders as shown in Figure 8a. This further indicates that spherical micelles come from the cylindrical micelles. An enlarged micrograph is inserted on the top right corner of Figure 8a. It is easy to know that the surface area per volume for a sphere is $A/V = 3/R$, where R, A and V are the radius, the total surface area and volume of the sphere, respectively. In the present study, the spherical micelle radius was $R = 22$ nm. Its surface area per volume A/V was 0.14 (nm^{-1}), which is larger than that of the long cylinders (the cylinder radius is 18 nm). The increase in the micelle surface (i.e., the micelle surface energy) results from the high stirring rate applied to the system. The transition from sphere to vesicle has been found both in experiments[30,31] and in theory.[32,33] The particular findings in the present study is that the vesicles formed were quite small. The inside radius for the vesicles was less than 35 nm. Stirring energy can be absorbed by a big aggregate in terms of kinetic energy (E_k) and potential (E_p). E_k can speed

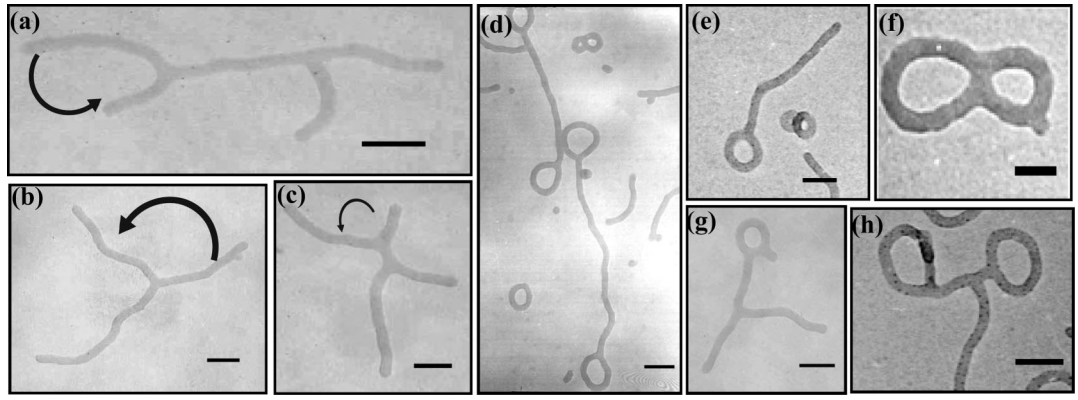

Figure 7. Intermediate structures trapped at a low stirring rate (200 rpm). The bars represent 100 nm.

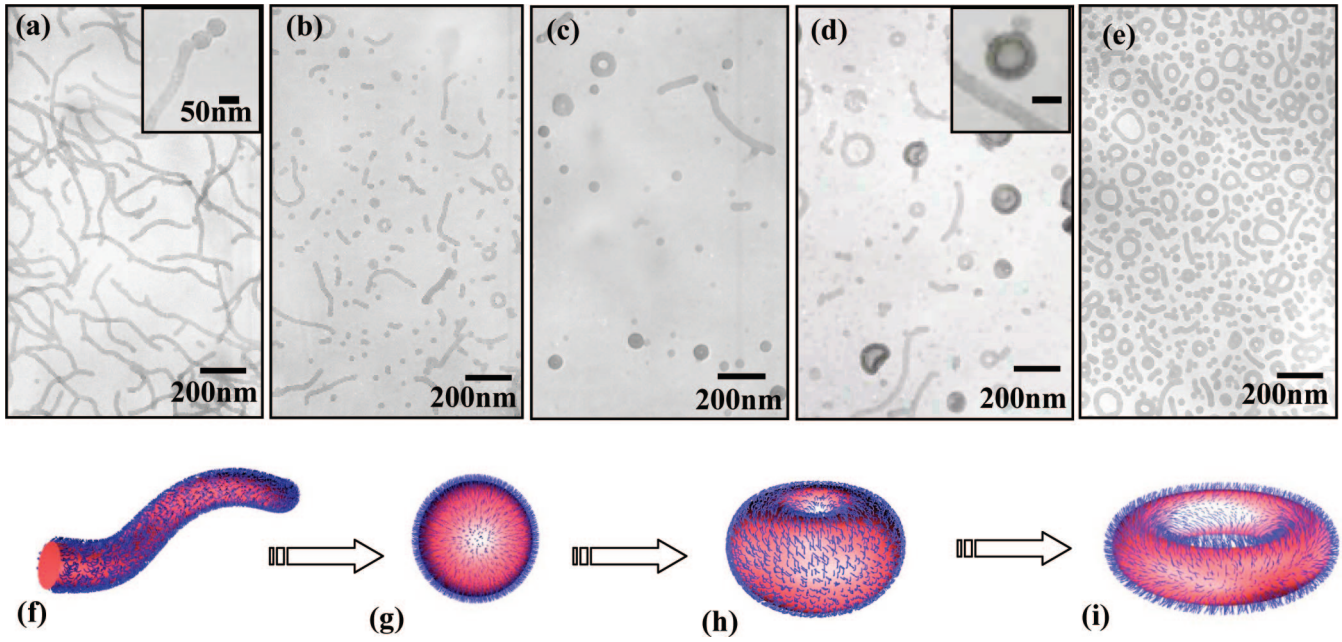

Figure 8. (a−e) Typical TEM images of the aggregate morphologies trapped at different annealing times at a high stirring rate (2000 rpm): (a) 5 min, (b) 1 h, (c) 10 h, (d) 15 h, and (e) 24 h. (f−i) Representations for ring formation via the rod−sphere−vesicle−ring process.

up the aggregate, whereas E_p can increase the internal energy of the aggregate, including deformation energy, and surface energy of the aggregate. Therefore, an increased stirring rate can be beneficial to the increase of the surface area of an aggregate if its surface tension remains unchanged. From this point of view, the big vesicle has some difficulty being formed under a high stirring rate condition due to its lower surface area per volume. The surface area per volume for a vesicle can be calculated from the following equation:

$$(A/V)_{vesicle} = \frac{3}{d} \times \left[\frac{2R^2 + 2dR + d^2}{3R^2 + 3dR + d^2} \right] \quad (1)$$

where R and d are the inside radius and wall thickness of a vesicle, respectively, and $d = 16$ nm in the present study. From eq 1 we can figure out that A/V drops rapidly with increasing R up to 35 nm; thereafter, it decrease slowly with increasing R. This may be the reason why there was some difficulty in observing the big vesicles (>35 nm) in the experiments. Nonetheless, it was revealed that the vesicles formed in the present system are in a metastable state.[34] They can break up to form ring micelles although the surface area per volume for the rings ($A/V = 2/r = 0.12$ nm^{-1}, the rod radius for the rings $r = 17$ nm) are smaller than that for the vesicles ($A/V = 0.15-0.13$ nm^{-1}). In the present study, the wall thickness of the vesicles was 16 nm. A vesicle with $R = 35$ can form a ring with the diameter = 132 nm. This ring size corresponded to the peak value for the ring size distribution at the stirring rate of 2000 rpm (Figure 3). This result further indicates that the small rings were from the breakdown of the vesicles. It is noteworthy that the ring-shaped micelles are quite stable. When stirring time was increased up to 20 d at 2000 rpm, the small rings remained unchanged.

Finally, it was discovered that rings with different sizes could be obtained at different stirring rates (Figure 2). Taylor's theory of the droplet break-up can be used to discuss the ring size controlling mechanism. It is known that the size (D_s) of emulsion droplets is largely controlled by the balance between the shear force and the interfacial tension, and D_s was given as[35,36]

$$D_s \approx \frac{\nu}{\eta_m \dot{\gamma}} \quad (2)$$

where η_m is the matrix phase viscosity (corresponding to the solution viscosity in the present study), $\dot{\gamma}$ is the applied shear rate, and ν is the interfacial tension between the two phases.

In our present work, long cylinders were initially formed from the self-assembly of the copolymer. Long cylinders (Figure 1a) cannot break-up without stirring. When stirring is applied, from eq 2 we can know that the higher the stirring rate is, then the shorter the cylinders are. As a result, increasing the stirring rate could have led to the decrease of ring size. However, sizable rings were difficult to find at a low stirring rate. This is because a very long or a very short cylinder is difficult to connect end-to-end, that is to say a cylinder with a moderate length is more likely to be connected via end-to-end, forming rings. As a result, sizable rings are difficult to be formed at a low stirring rate.

Conclusions

In conclusion, we wish to mention that stirring or shearing is generally used in micelle preparation. However, to the best of our knowledge, only a limited number of theoretical or simulative methods have been used to study micelle transition under shear flow. Shear flow is a key factor that determines the formation of rings. Both ring size and its distribution are found to be critically dependent on the stirring rate. Large rings are more likely to be formed at moderate stirring rates. Interestingly, the ring formation mechanism was also found to be dependent on shear flow. Copolymers were likely to form rings via end-to-end cylinder connection at low stirring rates, whereas they tended to form rings via the pathway of the rod−sphere−vesicle−ring process at high stirring rates. These findings enrich our knowledge of the potential for the self-assembly of amphiphiles under shear flow. We hope that our results provide motivation for related theoretical studies that may further aid the understanding of these phenomena.

Acknowledgment. Financial support was provided by the National Natural Science Foundation of China for General Program (20874099), Creative Research Groups (50621302), Outstanding Young Investigators (50725312), and the National Basic Research Program (2007CB808000) of China.

References and Notes

(1) Zhang, L. F.; Eisenberg, A. *Science* **1995**, *268*, 1728–1731.
(2) Walther, A.; Goldmann, A. S.; Yelamanchili, R. S.; Drechsler, M.; Schmalz, H.; Eisenberg, A.; Müller, A. H. E. *Macromolecules* **2008**, *41*, 3254–3260.
(3) Bai, Z.; He, Y.; Lodge, T. P. *Langmuir* **2008**, *24*, 5284–5290.
(4) Huang, H.; Remsen, E. E.; Kowalewsk, T.; Wooley, K. L. *J. Am. Chem. Soc.* **1999**, *121*, 3805–3806.
(5) Kim, B.; Park, S.; McCarthy, T. J.; Russell, T. P. *Small* **2007**, *3*, 1869–1872.
(6) Zhang, L.; Eisenberg, A. *Polym. Adv. Technol.* **1998**, *9*, 677–699.
(7) Zhu, J.; Jiang, W. *Macromolecules* **2005**, *38*, 9315–9323.
(8) Zhu, J.; Liao, Y.; Jiang, W. *Langmuir* **2004**, *20*, 3809–3812.
(9) Kataoka, K.; Harada, A.; Nagasaki, Y. *Adv. Drug Delivery Rev.* **2001**, *47*, 113–131.
(10) Adams, D. J.; Adams, S.; Atkins, D.; Butler, M. F.; Furzeland, S. *J. Controlled Release* **2008**, *128*, 165–170.
(11) Li, Y.-Y.; Zhang, X.-Z.; Kim, G.-C.; Cheng, H.; Cheng, S.-X.; Zhuo, R.-X. *Small* **2006**, *2*, 917–923.
(12) Pochan, D. J.; Chen, Z.; Cui, H.; Hales, K.; Qi, K.; Wooley, K. L. *Science* **2004**, *306*, 94–97.
(13) He, X.; Schmid, F. *Phys. Rev. Lett.* **2008**, *100*, 137802.
(14) van der Schoot, P.; Wittmer, J. P. *Macromol. Theory Simul.* **1999**, *8*, 428–432.
(15) In, M.; Aguerre-Chariol, O.; Zana, R. *J. Phys. Chem. B* **1999**, *103*, 7747–7750.
(16) Jain, S.; Bates, F. S. *Macromolecules* **2004**, *37*, 1511–1523.
(17) Léon, A.; Bonn, D.; Meunier, J.; AI-Kahwaji, A.; Kellay, H. *Phys. Rev. Lett.* **2001**, *86*, 938–941.
(18) Guo, H.; Kremer, K. *J. Chem. Phys.* **2007**, *127*, 054902.
(19) Balsara, N. P.; Hammouda, B. *Phys. Rev. Lett.* **1994**, *72*, 360–364.
(20) Koppi, K. A.; Tirrel, M.; Bates, F. S. *Phys. Rev. Lett.* **1993**, *70*, 1449–1452.
(21) Soos, M.; Moussa, A. S.; Ehrl, L.; Sefcik, J.; Wu, H.; Morbidelli, M. *J. Colloid Interface Sci.* **2008**, *319*, 577–589.
(22) Mahjoub, H. F.; Bourgaux, C.; Sergot, P.; Kleman, M. *Phys. Rev. Lett.* **1998**, *81*, 2076–2079.
(23) Yamamoto, J.; Tanaka, H. *Phys. Rev. Lett.* **1996**, *77*, 4390–4393.
(24) Zhang, L.; Eisenberg, A. *Macromolecules* **1999**, *32*, 2239–2249.
(25) Zheng, R.; Liu, G.; Yan, X. *J. Am. Chem. Soc.* **2005**, *127*, 15358–15359.
(26) Won, Y.-Y.; Davis, H. T.; Bates, F. S. *Science* **1999**, *283*, 960–963.
(27) Liu, G.; Yan, X. *Macromolecules* **2002**, *35*, 9788–9793.
(28) Croce, V.; Cosgrove, T. *Langmuir* **2003**, *19*, 8536–8541.
(29) Jung, Y.; Jung, W.; Ross, C. A. *Nano Lett* **2008**, *8*, 2975–2981.
(30) Zhang, L.; Eisenberg, A. *Macromolecules* **1996**, *29*, 8805–8815.
(31) Shen, H.; Zhang, L.; Eisenberg, A. *J. Am. Chem. Soc.* **1999**, *121*, 2728–2740.
(32) He, X. H.; Schmid, F. *Macromolecules* **2006**, *39*, 2654–2662.
(33) Yamamoto, S.; Maruyama, Y.; Hyodo, S. *J. Chem. Phys.* **2002**, *116*, 5842–5849.
(34) Jiang, Y.; Zhu, J.; Jiang, W.; Liang, H. *J. Phys. Chem. B* **2005**, *109*, 21549–21555.
(35) Taylor, G. *Proc. R. Soc. London, Ser. A* **1932**, *138*, 41–48.
(36) Taylor, G. *Proc. R. Soc. London, Ser. A* **1934**, *146*, 501–523.

MA900107R